

Modelling fission gas behaviour in fast reactor (U,Pu)O₂ fuel with BISON

Filippo Verdolin^a, Stephen Novascone^b, Davide Pizzocri^a, Giovanni Pastore^{b,c}, Tommaso Barani^a, Lelio Luzzi^a

^a*Politecnico di Milano, Department of Energy, Nuclear Engineering Division, via La Masa 34, I-20156 Milano, Italy*

^b*Computational Mechanics and Materials Department, Idaho National Laboratory, Idaho Falls, ID 83415, USA*

^c*Department of Nuclear Engineering, University of Tennessee, Knoxville, TN 37916, USA*

Abstract

The physics-based fission gas behaviour model available in the BISON fuel performance code provides satisfactory predictive capabilities for application to light-water reactor conditions. In this work, we present a model extension for application to fast reactor (U,Pu)O₂ fuel. In particular, we detail the introduction of a lower bound to the number density of grain-face bubbles, representing a limit to the coalescence process once extensive bubble interconnection is achieved. This new feature is tested first against an experimental database for UO₂-LWR, and secondly is validated against integral irradiation experiments for fast reactor (U,Pu)O₂ fuel rods irradiated in the FFTF (Fast Flux Test Facility) and in the JOYO reactors. The comparisons of BISON results with the experimental data are satisfactory and demonstrate an improvement compared to the standard version of the code.

Keywords: nuclear fuel, MOX, fast reactors, finite element method, fission gas behaviour

1. Introduction

Uranium-plutonium mixed oxide fuels (MOX) are candidate fuels for several fast reactor concepts [1, 2]. Fast reactor conditions pose (U,Pu)O₂ fuels under considerable load in terms of high-temperature, steep-temperature gradients and extended burnup [3, 1]. In view of this difference in the operation conditions, the behaviour of fission gas in fast reactor (U,Pu)O₂ fuels is different from that of UO₂ in light-water reactors (LWR). [4, 5, 6].

A sufficiently high-temperature gradient can induce the formation of a central void in the fuel pellet [3, 7]. The central void forms due to the migration up the temperature gradient of porosity left over from sintering [3, 7, 8]. Also, the migration of the pores leads to fuel restructuring, exhibiting the formation of new regions within the fuel. In particular, besides the central void, we can identify three other main regions within fast reactor (U,Pu)O₂ fuels (Fig. 1), characterized by different microstructures [7]:

- In the inner region of the fuel column where the temperature is high enough, the fuel undergoes restructuring driven by an evaporation/condensation mass transport across fabrication pores [3, 1, 9, 10]. In the restructured area, columnar grains are formed, exhibiting lower grain-boundary retention of fission gas than in the unstructured region because of the cylindrical shape of the columnar grains.
- In the intermediate region, after the restructuring, the microstructure of the fuel is characterized by equiaxed grains [3, 1].

- The outer region is unaltered. In this outer region, the pores do not move because of the low temperature.

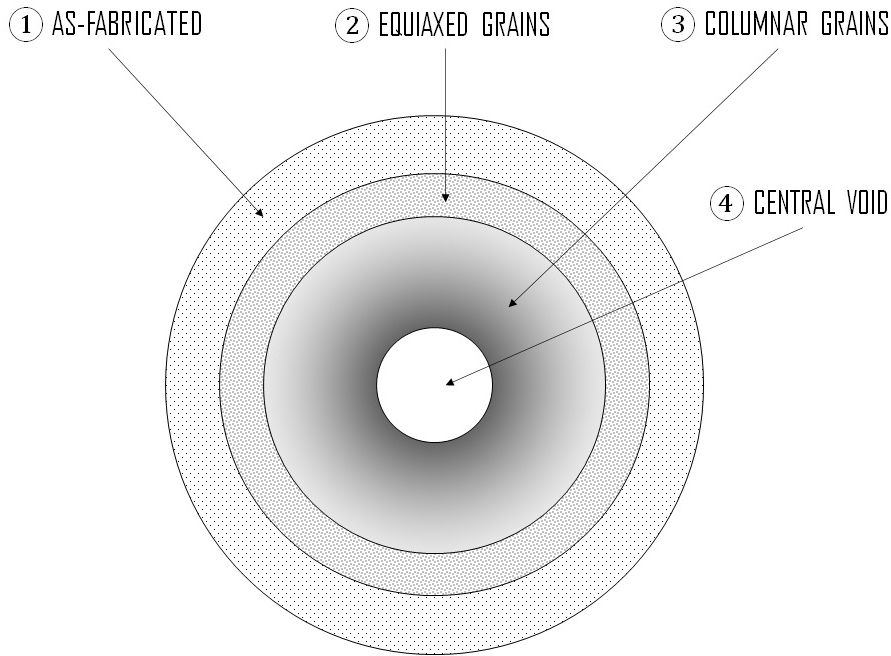


Figure 1: Diagram of microscale features where the region after restructuring are distinguished. For more detailed images and information, see Ref. [11].

Due to this difference in microstructure and in consideration of the high-temperature level in the fast reactor (U,Pu)O₂ fuel, attempting to directly apply fission gas behaviour models tailored to UO₂ in LWRs is usually not straightforward [12]. For example, difficulty arises from the fact that higher temperature implies (exponentially) faster kinetics of diffusive processes governing fission gas behaviour, resulting in a range of model solutions for fission gas release (FGR) and swelling typically not achieved in LWR conditions. It is worth noticing that conservative approaches assuming high temperatures and traditionally applied as design criteria are not acceptable predictive models to be applied in fuel performance simulations (e.g., used for the conservative design of the plenum free volume). It has been shown with best-estimate calculation (e.g., see Ref. [13]) that operational fission gas release in prototype lead-cooled and lead-bismuth-eutectic-cooled fast reactors is in the range of 20 to 60%, i.e., much higher than typical values for LWRs but well below the 80–90% observed in sodium-cooled fast reactors for power production [1]. Also, the range of 80–90% of release refers to past generations of sodium-cooled fast reactors, because of their higher temperature target, while, for the new generation sodium-cooled fast reactors, it is lower. On the other hand, Lead fast reactors (LFRs) and Lead Bismuth eutectic fast reactors (LBE-FRs) operates at lower temperatures; therefore, their FGR is also lower. For these reasons, the development of predictive models for fission gas behaviour in fast reactor (U,Pu)O₂ fuel is a key point for the effective application of fuel performance codes, hence, it is targeted by several research programs, like [14, 15, 16].

In this work, we present a version of the model by Pastore et al. [17, 18], which was originally developed and validated for LWR UO₂, adapted to the description of fission gas behaviour in fast reactor (U,Pu)O₂. In particular, we propose the introduction of a

66 physics-based limit to the process of coalescence of growing grain-boundary bubbles. We
 67 implemented the modified version of the model into the BISON fuel performance code [19]
 68 and we verified, for local ¹ analyses, the behaviour of this extension to the model against the
 69 experimental database presented by Baker [20, 21]. Subsequently, we validated the extended
 70 version of the model against integral irradiation experiment performed in fast reactors. It is
 71 worth noting that there are other phenomena linked to the FGR that do not depend strictly
 72 on the diffusion and the evolution of the gas bubbles, but they are connected to the fuel
 73 stoichiometry, the Plutonium content and species mobility. Also, the gas diffusion coefficient
 74 used in this work, i.e. Turnbull [22], may not be reliable because it has been developed for
 75 UO₂ at LWR conditions. For these reasons, we know that all these phenomena that are
 76 peculiar for (U,Pu)O₂ irradiated in fast reactors and the model of Pastore [18], tailored on
 77 UO₂ at LWR conditions, does not perceive. Therefore, the scope of this work is to show
 78 that a model for fission gas behaviour developed for LWR conditions with few improvements
 79 could have a good reproducibility of the results for (U,Pu)O₂ irradiated in fast reactors.
 80 However, this work represents an initial extension and other important phenomena that
 81 affect FGR (like stoichiometry, Plutonium content, species migration) will be considered in
 82 future work.

83 The outline of this paper is as follows. In Section 2, we briefly summarize the main model
 84 equations and we detail the proposed modifications. In Section 3, the modified model is
 85 tested for local analyses of UO₂ fuel irradiation at temperatures covering both LWR and
 86 FBR (Fast Breeder Reactor) ranges. In Section 4, the modified model is tested for the
 87 simulation of integral irradiation experiments under fast reactor conditions with BISON,
 88 and results are compared to experimental data.

89 2. Model description

90 In this section, we briefly summarize the main model equations and we detail the pro-
 91 posed modifications. In the second part, we discuss some fundamental assumptions and
 92 parameters that affect the simulated fission gas behaviour.

93 2.1. Model development

According to the model of Pastore et al. [17, 18] fission gas behaviour is described as
 comprised of two main components, i.e., the intra-granular and inter-granular stages. The
 intra-granular part of the model can be summarized as follows.

Fission gas atoms generated in the fuel grains diffuse towards the grain boundaries through
 the processes of trapping into and re-solution from nanometer-size intra-granular gas bub-
 bles. The gas arriving at the grain-faces precipitates into grain-face gas bubbles, responsible
 for grain-face swelling. Fission gas diffusion from within the fuel grain (assumed as spheri-
 cal) to the grain boundary in one-dimensional spherical geometry is described by:

$$\frac{\partial C}{\partial t} = D_{\text{eff}} \frac{1}{r^2} \frac{\partial}{\partial r} \left(r^2 \frac{\partial C}{\partial r} \right) + \beta \quad (1)$$

94 where C (atoms m⁻³) is the intra-granular gas concentration (as single atoms in dynamic
 95 solution with the matrix and in bubbles), t (s) is the time, r (m) is the radial coordinate in

¹With local analysis and simulation, we mean a simulation using a simplified fuel-only model with a
 single-cube mesh, in order to simulate the local behaviour of the model in small fuel samples.

96 the spherical geometry, β (atoms $\text{m}^{-3} \text{s}^{-1}$) is the gas generation rate, D_{eff} ($\text{m}^2 \text{s}^{-1}$) is the
 97 effective gas diffusion coefficient from Speight [23].

98

The inter-granular part of the model involves the concurrent calculation of gaseous fuel swelling due to grain-face bubbles and fission gas release, through a description of grain-face bubble development [17, 18]. In summary, an initial number density of grain-face bubbles, N_0 (bubbles m^{-2}), is considered with further nucleation during irradiation being neglected (one-off nucleation). Bubbles are assumed to have lenticular shape of circular projection on the grain faces and to all have the same size at any instant. The absorption rate of gas atoms at bubbles is considered to equal the arrival rate at grain boundaries from Eq. 1. The phenomenon of growth (or shrinkage) of grain-face bubbles is described by Pastore et al. [17] referring to the model of Speight and Beere [24]. The overpressurization of the gas bubbles is the driving force of the vacancy absorption/emission mechanism:

$$\frac{dn_v}{dt} = k(p - p_{\text{eq}}) \quad (2)$$

where n_v (vacancies bubble^{-1}) is the number of vacancies per bubble, k is a kinetic constant depending (exponentially) on temperature and on the geometry of the grain face (see White [25]), p and p_{eq} (Pa) are the pressure of the gas in the bubble and the mechanical equilibrium pressure, respectively. The gas pressure is calculated based on the number of gas atoms and vacancies in each bubble and using the van der Waals equation of state [17]. Bubble growth leads the grain-face bubbles to interconnect and merge into larger but fewer bubbles. This coalescence process is described, using a modified model of White [25], relating the rate of decrease of the bubble number density, N (bubble m^{-2}), due to coalescence to the rate of increase of bubble projected area on the grain-face, A (m^2)

$$\frac{dN}{dt} = \frac{6N^2}{3 + 4NA} \left(\frac{dA}{dt} \right) \quad (3)$$

Hence, the coalescence process results in progressively fewer, larger bubbles. When the bubbles reach a sufficient level of interconnection, the grain face is considered as percolated and the fission gas is released to the fuel rod free volume through free pathways made of interconnected bubbles. In the model of Pastore et al. [17], this is underpinned by a principle of grain-face saturation: after the fractional coverage $F = NA$ has reached the saturation value F_{sat} , further bubble growth is compensated by gas release in order to maintain the constant coverage condition:

$$\begin{aligned} \frac{dn_{\text{FGR}}}{dt} &= 0 \quad \text{if } F < F_{\text{sat}} \\ \frac{dn_{\text{FGR}}}{dt} &= n \frac{N}{A} \frac{dA}{dt} \quad \text{if } F = F_{\text{sat}} \end{aligned} \quad (4)$$

99 where n_{FGR} (atoms m^{-2}) is the number of gas atoms released to the fuel rod free volume per
 100 unit grain-boundary surface and n (atoms bubble^{-1}) the number of fission gas atoms per
 101 grain-face bubble. The saturation point is assumed as a constant with a value of $F_{\text{sat}} = 0.5$
 102 [25, 17, 18].

103 The model by Pastore et al. [17] is currently the default option in BISON [19], and
 104 has been extensively validated in LWR UO_2 cases [17, 18, 26, 27]. It is expected that for
 105 $(\text{U,Pu})\text{O}_2$ fuels irradiated in fast reactors this model requires modifications and further
 106 validation.

107 In fact, it has been demonstrated [5, 28] that fission gas release reaches high values
 108 (outside of the current validation range of the model) at high temperatures often achieved
 109 by (U,Pu)O₂ fuels irradiated in fast reactors. In these conditions, the kinetic constant k in
 110 Eq. 2 becomes large, resulting in bubbles rapidly growing by diffusion-driven absorption of
 111 gas atoms and vacancies. As a consequence of bubble growth, the bubble number density
 112 strongly decreases, governed by Eq. 3.

113 Nevertheless, there should be a physical limit to the coalescence process, i.e., bubble
 114 growth would not result in noticeable further reduction of the number of bubbles once ex-
 115 tensive interlinkage is attained. In a simple approach, this limit can be interpreted as a
 116 lower bound to the number density of grain-face bubbles. In the original BISON model,
 117 such a lower bound was set to a constant value of 10^{10} bubbles m⁻² [18]. However, this
 118 limit is of low importance for LWR fuel calculations, where it is normally not attained. On
 119 the contrary, for the analysis of higher temperature fuel such as (U,Pu)O₂ fuels irradiated
 120 in fast reactors in which bubble growth and coalescence proceed more rapidly, the limit
 121 becomes highly important in determining the calculated FGR and gaseous swelling.

122

123 In this work, we further develop the concept of a lower bound for the number density
 124 of grain-face bubbles and propose a physically grounded approach to its determination.

Assuming a spherical grain of radius a (m), it has a surface area of $4\pi a^2$ (m²). Idealizing
 the surface area as divided into a number of grain faces n_{face} , each face has an area of

$$A_{\text{face}} = \frac{4\pi a^2}{n_{\text{face}}} \quad (5)$$

Considering that each grain face is shared by two grains, and considering a number of
 equivalent bubbles per grain face n_{eq} , we can express the bubble number density as

$$N = \frac{1}{2} \frac{n_{\text{eq}}}{A_{\text{face}}} = \frac{1}{2} \frac{n_{\text{eq}} n_{\text{face}}}{4\pi a^2} \quad (6)$$

With this notation, the limit number density of grain-face bubbles per unit surface, N_{lim}
 (bubbles m⁻²) is

$$N_{\text{lim}} = \frac{1}{2} \frac{n_{\text{eq,lim}} n_{\text{face}}}{4\pi a^2} \quad (7)$$

125 where $n_{\text{eq,lim}}$ (bubbles face⁻¹) is the average number of bubbles on a grain face when the
 126 saturation of bubbles is reached. The estimation of this parameter is obtained via a random
 127 numerical experiment detailed in the following subsection. As for the number of faces per
 128 grain n_{face} , it is assumed to be 14, based on the number of faces of a tetradecahedron.

129 2.2. Random numerical experiment for the derivation of the bubble equivalent number

130 In this section, we describe the process used for the derivation of the bubble equivalent
 131 number, $n_{\text{eq,lim}}$. In order to determine a range of reasonable values for the bubble equivalent
 132 number, we performed a numerical experiment. The goal of this experiment is just the
 133 derivation of the bubble equivalent number and not the bubble evolution itself because we
 134 are aware of the limitations of this derivation in describing such a complex phenomenon.

135 This numerical experiment presents the following characteristics:

- 136 • We generate 1000 square images representative of the grain-faces.
- 137 • Each grain face is assumed of size $10 \times 10 \mu\text{m}^2$.

- 138 • On each grain face, we generate overlapping single-sized circles of radius R sampled
139 from an uniform distribution $R(\mu\text{m}) \sim \mathcal{U}[0, 1]$.
- 140 • In each grain face, we count the effective number of bubbles, i.e., the number of
141 not-connected clusters of circles.

142 For this numerical experiment, we considered that the exact size of the grain face is not
143 relevant for the determination of the proposed lower bound to bubble number density since
144 it is expressed in terms of density². Nevertheless, the assumed size of the grain face cor-
145 responds to a grains radius of 10 μm . This can be determined by approximating the 3D
146 shape of the grain with a sphere of surface $4\pi a^2$. If one assumes it is divided into 14 faces
147 of 100 μm^2 each, a corresponds to a value of 10 μm .

148 Also, both bubbles centres coordinates are sampled from uniform distributions. Bubbles
149 ending up close to the edge are simply trimmed by the edge. We are not interested in
150 catching edge-effects, such as percolation of the grain face, and hence the shape of the edge
151 does not represent a strong limitation to our conclusion.

152 In principle, given enough trials, the patterns generated with bubbles of different size will
153 be covered also by single-size bubbles (with a higher number of smaller single-size bubbles,
154 i.e., the increase in trials required).

155 We are aware that overlapping circles is a partial representation of bubble coalescence,
156 missing the relaxation of edges which could be represented by phase-field models [29, 30].
157 On average, both the phase field and the overlapping circles are a reasonable representation
158 of the experimental data³.

159
160 In Figure 2a, the effective number of bubbles is reported as a function of the fractional
161 coverage F , with each point representing one of the 1000 images generated. The number
162 of effective pores gradually decreases with the increase of the fractional coverage, because
163 of coalescence. As an example, Figure 2b reports one of the images generated, with frac-
164 tional coverage $F = 0.43$ and a number of effective bubbles $n_{\text{eq}} = 29$. From Figure 2a,
165 in conditions of saturation, i.e., when $F = F_{\text{sat}} = 0.5$, n_{eq} is in the range 0-20 bubbles
166 face⁻¹. In this work, we assume⁴ $n_{\text{eq,lim}} = 10$. Moreover, comparing N_{lim} with the range
167 observed bubble densities at saturation, one can note that the proposed limit in this work
168 is compatible with experimental observations of saturated grain boundaries⁵, see Ref. [25].
169

²This assumption holds if the square is big enough compared to the bubble size.

³This comparison is performed on the vented fraction, and we are careful in claiming its generality, but we believe it is an indication of the viability of our “geometrical” approach.

⁴It should be clarified that the bubble concentration we are considering in our model is independent on the grain size, whereas the absolute number of bubbles is consequently proportional to the grain surface area. This assumption is justified by the fact that we do not consider grain growth and therefore the grain size of the problem is fixed as an initial condition. This modelling choice arises from the fact that classical grain growth models are barely applicable in the temperature range of the fuels considered in this work. This implies that the resulting “grain size” referred to in our work is more a modelling abstract quantity than a physical variable representative of the real grain size.

⁵The values for N_{lim} used in sections 3 and 5 fall in the range of 0.9–270×10¹¹ bubbles m⁻² observed by White [25]. It is important to keep in mind that the values of N_{lim} (from 5.6×10¹⁰ bubbles m⁻² to 3.5×10¹¹ bubbles m⁻² for a grain radius of 10 and 4 μm , respectively) are related to saturation conditions, i.e. at a fractional coverage of 0.5 because this model feature becomes relevant when the saturation of grain boundaries has been reached. However, the data by White [25] are taken from fuel irradiated and ramped in conditions which may not be representative of a fast reactor environment, therefore we are inclined to consider this comparison as indicative and not a strong support of the proposed new parameter.

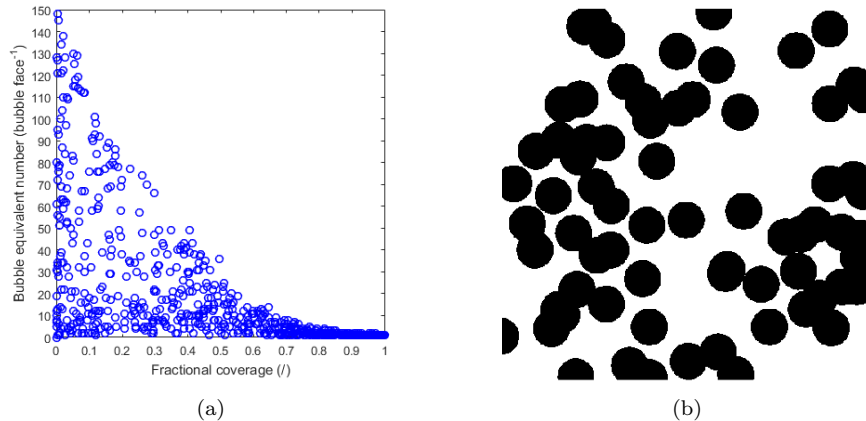


Figure 2: Results of the random numerical experiment used to derive the number of equivalent bubbles per grain face. On the left (a) we report the bubble equivalent number obtained as a function of the fractional coverage, while on the right (b) we report a sample image of a pattern of bubbles covering a grain face as obtained by the random process.

170 The inclusion in the BISON fission gas behaviour model of a lower bound to the inter-
 171 granular bubble density bounds the coalescence process and, once the lower limit for the
 172 number density of bubbles is achieved, any further bubble growth is compensated by FGR
 173 by virtue of Eq. 4, and both bubble number density and size remain constant. Note that in
 174 the current model, given the same fractional coverage, the fewer the bubbles the larger the
 175 volume they occupy and the higher the total gas atoms they retain [17, 18]. Hence, FGR
 176 after the attainment of the limit is expected to be higher compared to the situation where
 177 coalescence continues.

178 After the attainment of the lower limit in the number density of grain-face bubbles,
 179 in the model, the grain-face bubble population is assumed to reach a stationary situation
 180 where further evolution is prevented. Also, after extensive interlinkage, bubbles form elon-
 181 gated or vermicular structures [25], so that the basic model assumption of circular bubbles
 182 becomes stronger in itself. However, the concept of a stationary situation is considered
 183 reasonable as an attempt to consider behaviour after extensive bubble interlinkage within
 184 the current model framework and in a physically meaningful way. As a final physical justi-
 185 fication for the introduction in the model of such a lower bound, it should be observed that
 186 without any limitation the evolution of grain-face bubbles ignores the fact that bubbles are
 187 constrained on a single grain face, and can in principle allow for interconnection between
 188 bubbles belonging to different grain faces.

189 2.3. Modeling assumptions and parameters

An important parameter that affects FGR is the single gas atom diffusion coefficient. The default intra-granular single gas atom diffusion coefficient used in BISON standard version was provided by Turnbull et al. [31] neglecting the contribution of the athermal term (D_3). However, for the simulations with the extended model, we decided to use the single gas atom diffusion coefficient proposed by Turnbull et al. [22]. We decided to use the original complete diffusion coefficient proposed by Turnbull [22] as it is since it is the reference coefficient used in most similar models in the state of the art. This diffusion coefficient is described as follows:

$$D_s = D_1 + D_2 + D_3 \quad (8)$$

190 where D_1 ($\text{m}^2 \text{s}^{-1}$) is the thermal component that depends just on temperature, D_2 ($\text{m}^2 \text{s}^{-1}$)
191 the irradiation-enhanced term that is a function of both temperature and the fission rate
192 and D_3 ($\text{m}^2 \text{s}^{-1}$) is the athermal component depending only on the fission rate. It has been
193 decided to use the coefficient proposed by Turnbull et al. [22] because this diffusion coef-
194 ficient emphasizes the enhanced and the athermal components dependent on the fission rate.

195

196 In addition, another issue related to the simulation of fast reactor (U,Pu)O₂ cases with
197 BISON pertains to the grain growth. BISON only incorporates an UO₂-LWR model [32],
198 which is not suitable to represent grain growth under FBR conditions. Hence, for this
199 work, because of the lack of a model able to describe the grain growth for these conditions,
200 it has been decided to use constant values for the grain radius⁶. We are aware that the
201 restructuring of oxide fuel in fast reactor conditions determine a dramatic change in the
202 crystalline structure [3, 9], as mentioned in the introduction of this work. Indeed, the
203 inclusion of a consistent model for grain growth, fuel restructuring and their influence of
204 fission gas behaviour will be the subject of future investigations.

205 An investigation about the effects of the grain radius on the limit described in Eq. 7 is
206 performed in Section 5.

207 3. Model test with local simulations with BISON

208 In this section, we assess the impact of the lower bound of bubble number density
209 introduced via Eq. 7 on the fission gas behaviour model of Pastore et al. [17, 18] at
210 different temperatures. The assessment is carried on analyzing the experimental database
211 from Baker (Ref. [21, 20]). In these experiments, the fuel pins have been irradiated in the
212 UKAEA's Winfrith SGHWR up to a burnup of $\sim 1\%$ and the samples examined by Baker
213 (Ref. [21], [20]) lay in the temperature range from 1273 K up to 2073 K. Therefore, these
214 values represent both operational conditions for UO₂-LWR (up to about 1600 K) and more
215 critical ones (beyond 1700 K), closer to operational conditions of (U,Pu)O₂ fuel irradiated
216 in fast reactors.

217 The experimental data from [21, 20] correspond to local information, i.e., small fuel
218 samples from irradiated rods. In order to simulate local behaviour with BISON, we used a
219 single-cube mesh. Every simulation has been performed at a different temperature (starting
220 from 1273 K up to 2073 K, consistent with the Baker database) and assuming a typical
221 value⁷ for the grain radius, i.e., 5 μm , corresponding to a N_{lim} of 2×10^{11} bubbles m^{-2} ,
222 coming from Eq. 7.

223 Figures 3 and 4 report all the results at each of the considered temperatures for the
224 quantities of most interest, namely: the fission gas release FGR (%), the number density
225 of grain boundary bubbles per unit surface N (bubbles m^{-2}) and the volumetric swelling
226 due to grain-boundary bubbles (%). The results are shown for both standard and modified
227 BISON. At lower temperatures (Fig. 3), since the bubble number density at the grain
228 boundaries N does not reach the proposed limit N_{lim} , the resulting FGR and volumetric
229 swelling at the grain boundary are the same in both the cases. In Fig. 4, as temperature
230 raises (from 1773 K and so on), the lower bound for the bubble number density at the

⁶We assumed the grain radius as constant in time and uniform along the pellet radius. This abstract modelling assumption is to be intended just for the modelling of fission gas behaviour and should not be intended as a general model representative of the fuel microstructure.

⁷This consideration might be correct for equiaxed grains, but here we are not considering the cylindrical grains.

231 grain boundary proposed in this work is attained (Figs. 3a, 3d, 3g and 3j) and this implies
232 a higher *FGR* and a lower volumetric swelling at the grain boundary compared to the
233 standard BISON case.

234 The swelling prediction we observe at high temperature is higher than that observed by
235 White [25]. This is to be expected, since the irradiation histories which end up with swellings
236 around 7% are the result of 5'500 hours of irradiation at 1800°C, while the irradiations
237 considered by White are characterized by slightly higher temperatures but only for ramps of
238 short duration. The irradiation time at high temperature is the principal reason behind the
239 difference in the two values of swelling. In fact, due to the higher temperatures (comparable
240 to ranges for fast reactor (U,Pu)O₂ fuel), the associated pronounced bubble growth and
241 coalescence lead to the attainment of the lower bound for the number density of grain
242 boundary bubbles systematically.

243 These results highlight the impact of the proposed model modification at temperatures
244 comparable to fast reactor fuel conditions.

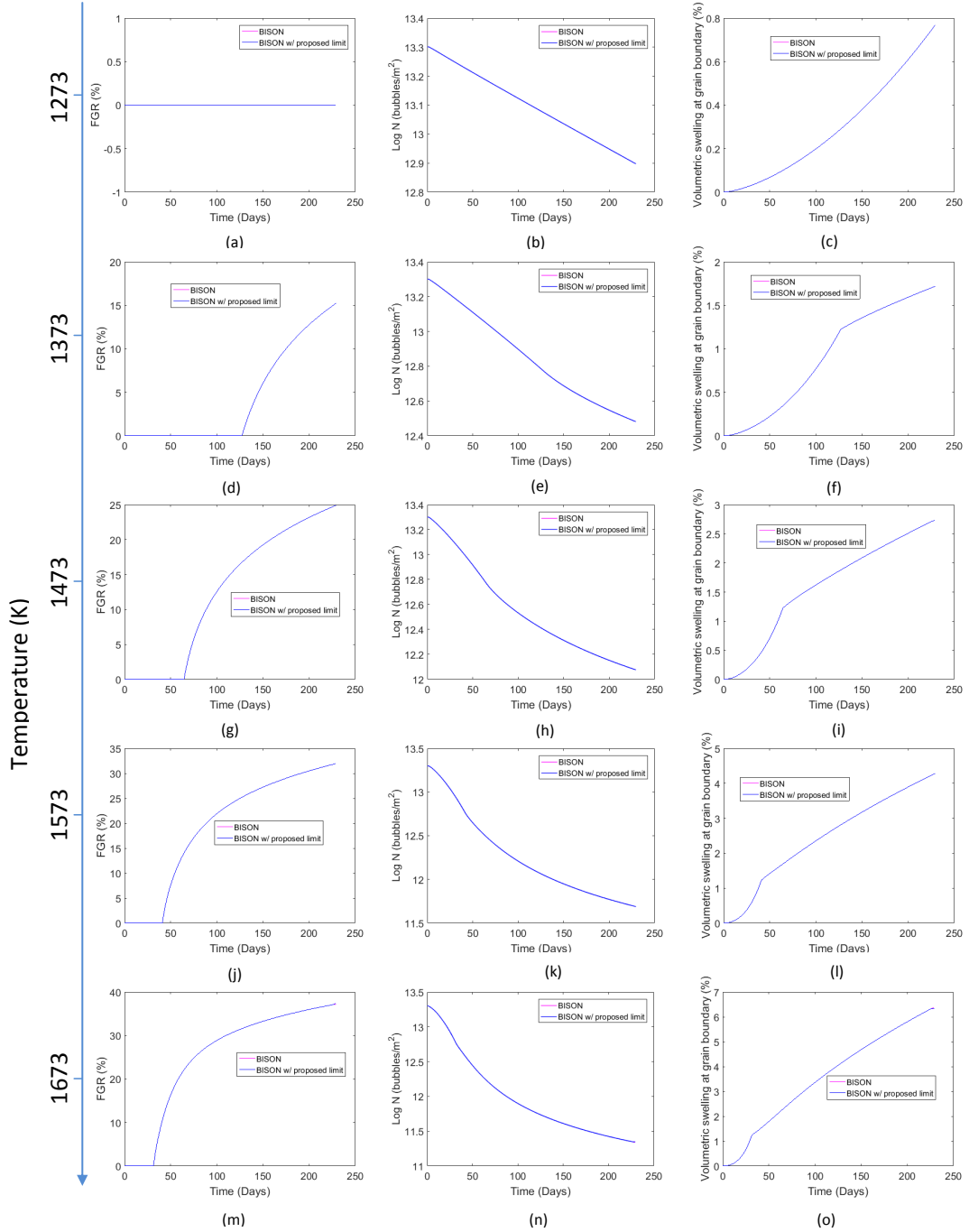


Figure 3: Local simulations on UO_2 from the Baker database ([21] and [20]) performed with BISON in a range of temperatures from 1273 K up to 1673 K. For every temperature the fission gas release FGR (%), the number density of bubbles at the grain boundary per unit surface N (bubbles m^{-2}) and the volumetric swelling at the grain boundary (%) evolution as a function of the time are reported. The plots related to N are expressed with a semi-logarithmic scale. In every figure, the purple lines, corresponding to the standard BISON version, cannot be distinguished from the blue ones (with a N_{lim} of 2×10^{11} bubbles m^{-2} , coming from Eq. 7), because they are overlapped.

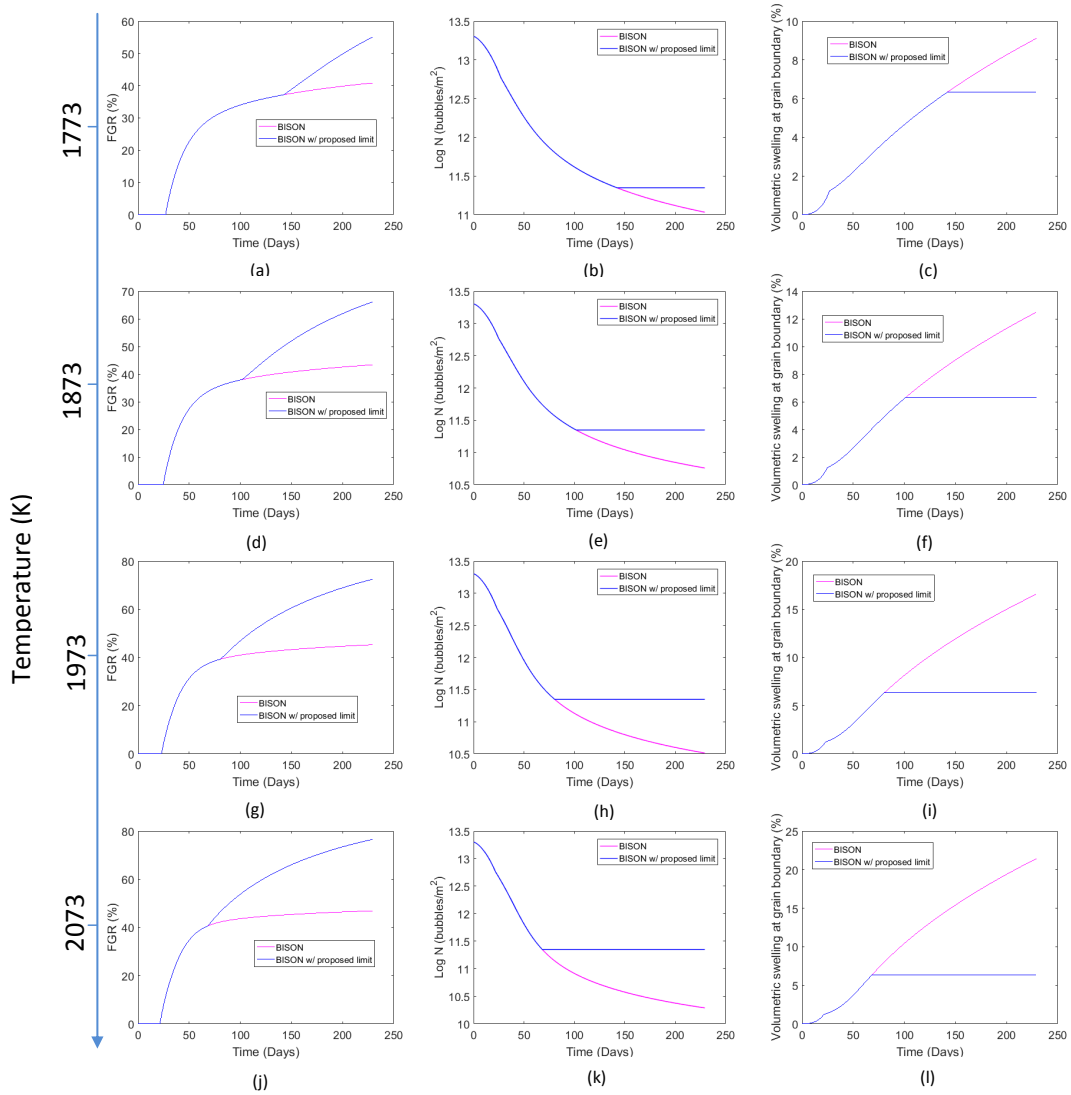


Figure 4: Local simulations on UO_2 from the database [21] and [20] performed with BISON in a range of temperatures from 1773 K up to 2073 K. For every temperature the fission gas release FGR (%), the number density of bubbles at the grain boundary per unit surface N (bubbles m^{-2}) and the volumetric swelling at the grain boundary (%) evolution as a function of the time are reported. The plots related to N are expressed with a semi-logarithmic scale in order to highlight the differences between the two cases analyzed. The purple line refers to the standard BISON version; the blue line refers to the case that uses the lower bound for the bubble number density at the grain boundary N_{lim} (Eq. 7), corresponding to a value of 2×10^{11} bubbles m^{-2} .

Table 1: Fuel pin specifications and irradiation data.

Rod	FO-2 L09	MK-I at 50MW _t	MK-I at 75MW _t	MK-II
Fuel Data				
Fuel material	(U,Pu)O ₂	(U,Pu)O ₂	(U,Pu)O ₂	(U,Pu)O ₂
PuO ₂ content (wt%)	26.0	18	18	30
Pellet outer diameter (mm)	5.59	5.4	5.4	4.63
Pellet inner diameter (mm)	1.397	-	-	-
Fuel stack height (mm)	914	600	600	550
Pellet density (%TD)	91.7	93.5	93.5	93
Fuel Rod				
Cladding material	HT-9	316SS	316SS	316SS
Cladding outer diameter (mm)	6.858	6.3	6.3	5.5
Cladding thickness (mm)	0.533	0.35	0.35	0.35
Gap width (μm)	101.6	100	100	100
Nominal plenum height (mm)	1057	600	600	550
Fill gas composition	He	He	He	He
Fill gas pressure (MPa)	0.1	0.3	0.3	0.3
Linear heat rate (kW m ⁻¹)	38.8 ⁸	21	32	40
Max. Burnup (% FIMA)	~6	~2.5	~5	~5

245 4. Integral fuel rod analyses

246 The integral irradiations simulated⁹ in the present work are taken from the experiments
247 FO-2 [33, 34], MK-I and MK-II [35]. The FO-2 assembly has been irradiated in the Fast Flux
248 Test Facility (FFTF), a sodium fast reactor, for 312 equivalent full power days (EFPD) [33]
249 between December 22, 1984, and April 25, 1986, to a peak burn-up of ~6% FIMA (Fissions
250 per Initial Metal Atom) and a peak fast fluence of 9.9×10^{22} n cm⁻² ($E > 0.1$ MeV) [34].
251 This test uses the alloy HT-9 as cladding material. The FO-2 assembly is composed by
252 169 fuel pins of twelve different types. The fuel was manufactured with co-precipitated
253 (U,Pu)O₂ powder, ensuring a uniform plutonium distribution throughout the pellets [34].
254 The annular fuel¹⁰ pin L09 was destructively examined. This pin was punctured and it was
255 cut at three different elevations.

256 JOYO was the first sodium-cooled reactor leading the FBR development program in Japan.
257 MK-I core has been irradiated in the Japanese experimental fast reactor JOYO at 50 MW_t
258 and at 75 MW_t from 1977 to 1981 [35], up to a burnup of ~2.5% FIMA and ~5% FIMA,
259 respectively. MK-II core was irradiated in the JOYO reactor from 1983 to 1986, up to a
260 burnup of ~5% FIMA. The MK-I and MK-II cores are composed by a maximum of 80 and
261 67 driver assemblies, respectively, surrounded by stainless steel reflectors.

262 More details about the power histories and other information for the experiments FO-2
263 and MK can be found in Teague et al. [34] and Shimada et al. [35], respectively. The
264 specifications for these experiments are summarized in Table 1.

⁸The provided power refers to a simplified power history from Teague et al. [34] and it is representative of the average value.

⁹Phenomena like oxygen defects are outside of the scope of this work, although their impact on the overall behaviour of fast reactor fuel and on fission gas behaviour is relevant.

265 **5. Calculation results**

266 In this section, we show the results of integral rod simulations and a sensitivity analysis
267 about the impact of the grain size on the results.

268 *5.1. Integral rod simulation results*

269 In this Section, we present the calculation results of integral rod simulations obtained
270 with BISON. In Figs. 5a-5d two different cases have been examined:

- 271 • A first one that considers the standard version of BISON;
- 272 • A second case that takes into account the lower limit for the bubble number density
273 at the grain boundary N_{lim} (Eq. 7) dependent on the grain radius proposed in this
274 work with the single gas atom diffusion coefficient presented by Turnbull et al. [22].

275 As shown in Figs. 5a-5d, one can observe that introducing N_{lim} according to Eq. 7 the
276 fission gas release prediction is closer to the experimental data. These results indicate that
277 the limitation introduced describes better the physical limit of grain-face bubble intercon-
278 nection occurring at typical operational conditions for fast reactor (U,Pu)O₂ fuel. However,
279 in some cases, the results are not in a good agreement with the experimental data (e.g Fig.
280 5b at a burnup lower than 1% FIMA). In this case, the onset is not well described by the
281 model. The reason could be because further modelling developments are required to take
282 into account other phenomena (like stoichiometry and Plutonium content and distribution)
283 that affect the FGR.

284 Also, the quality of the results could be affected by the use of some parameters that have
285 been developed for LWR conditions, first of all, the gas diffusion coefficient. The relation-
286 ship provided by Turnbull [22] could not be enough accurate to describe this phenomenon
287 under such different conditions (e.g. higher temperatures, different microstructure, different
288 stoichiometry).

289
290 In order to discuss the effect of grain-size on the results, we propose a sensitivity analysis
291 with an analytical approach. This analysis was performed concerning the model illustrated
292 by Pastore et al. [17, 18].

293
294 *5.2. Sensitivity Analysis*

In this section, we want to add more value to our work, performing a sensitivity analysis
study. However, the sensitivity analysis is not the main goal of this work, and this study
will be investigated more deeply in future publications. To see the effects on the final
release due to the perturbation, generated adding a quantity δC of gas¹¹, it is necessary
to linearize¹² the equations (presented by Pastore et al. [17, 18] and seen in Section 2)
that govern the fission gas behaviour. Hence, once linearized, Eq. 1 that describes the
intra-granular diffusion becomes:

$$\frac{\partial \delta C}{\partial t} = D_{\text{eff}} \frac{1}{a} \frac{\partial^2 \delta C}{\partial r^2} \Big|_a \quad (9)$$

¹⁰Furthermore, the effect of open porosity, due to an annular pellet or to the formation of a central void,
is not taken into account because the fission gas behaviour model implemented in BISON operates by point.

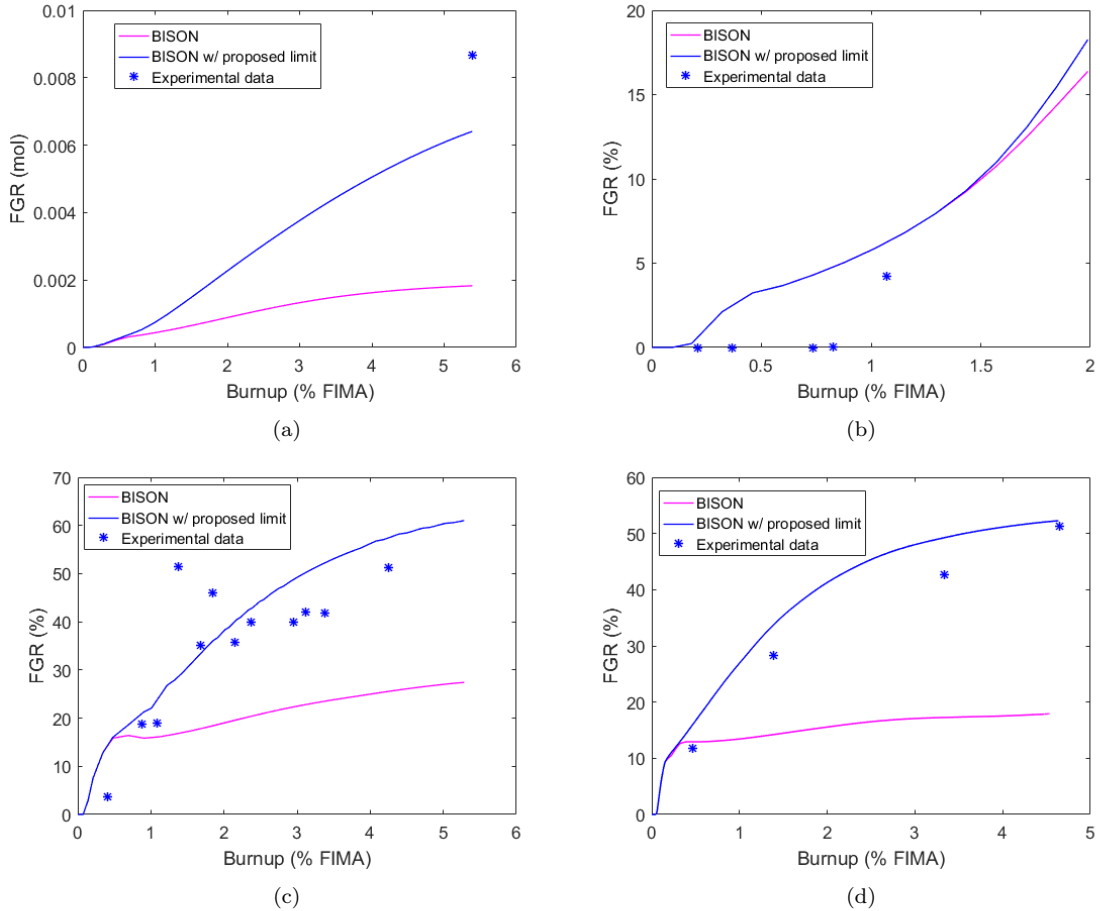


Figure 5: Calculation results for FGR compared with experimental irradiation data. The purple line refers to the standard BISON version; the blue line corresponds to the case that uses the lower limit for the bubble number density at the grain boundary N_{lim} (Eq. 7). Fig. 5a refers to the fuel pin L09 from the FO-2 assembly, assuming a constant grain radius of 10 μm , value reported by [34]. The consequent N_{lim} corresponds to a value of 5.6×10^{10} bubbles m^{-2} . Figs. 5b-5c show the results for MK-I core irradiated at 50 MW_t and at 75 MW_t respectively, while the simulations for MK-II core are illustrated in Fig. 5d. Figs. 5b-5d, related to JOYO reactor, refer to a constant grain radius of 8 μm [36], with N_{lim} corresponding to a value of 8.7×10^{10} bubbles m^{-2} .

295 Eq. 9 shows an inverse proportionality between the diffusion phenomenon and the grain
 296 radius a . In fact, the larger the grain, the longer the average diffusion path to the grain
 297 boundary.

298

After linearizing all the equations governing the grain boundary gas behaviour (Eqs. 2-4) presented by Pastore et al. [17], referring to the fractional coverage $F = F_{sat} = 0.5$ (/) as stationary steady-state point and adding a δC as perturbation to the system, one

¹¹The scope of the model is limited to fission gas behaviour and does not consider several fundamental effects yet, which are therefore not included in the sensitivity.

¹²The overall model is highly non-linear, and linearization is to be done carefully. In our analysis, the linearization is to be intended in the proximity of a set of the state variables of the model and used only for perturbation purpose. In the proximity of the set of state of variables values, the linearization is thus a legitimate approximation.

obtains:

$$\delta n_{\text{FGR}} \Big|_{N_{\text{lim}}} = \frac{n_{\text{sp}} N_{\text{sp}}}{A_{\text{sp}}} \left[\left(\omega + \frac{2\pi D_v \delta_g t}{\Omega S n_{\text{vsp}}} \right) \left(\frac{\delta C}{3N_{\text{sp}}} a \right) \right]^{2/3} \quad (10)$$

where δn_{FGR} (atoms m^{-2}) is the variation of number of fission gas atoms released to the fuel rod free volume after the perturbation, assuming a constant value of N_{lim} , n_{sp} (atoms bubble^{-1}) is the number of fission gas atoms per grain-face bubble in the stationary point, N_{sp} (bubbles m^{-2}) is number density of grain-face bubbles per unit surface in the stationary point, A_{sp} (m^2) is the projected area of grain-face bubbles, ω (m^3) is the van der Waals' volume of a fission gas atom, D_v ($\text{m}^2 \text{s}^{-1}$) is the vacancy diffusion coefficient on grain boundaries, δ_g (m) is the thickness of the diffusion layer in grain boundaries, Ω (m^3) is the atomic (vacancy) volume in grain-boundary bubbles, S (-) is a model parameter (that depends on the fractional coverage) calculated in Pastore et al. [25], n_{vsp} (vacancies bubble^{-1}) is the number of vacancies per grain-face bubble in the stationary point, and t (s) is the time. Performing a derivative of Eq. 10 with respect to the grain radius a , one can obtain:

$$\frac{\partial \delta n_{\text{FGR}}}{\partial a} \Big|_{N_{\text{lim}}} = \frac{n_{\text{sp}} N_{\text{sp}}}{A_{\text{sp}}} \left[\left(\omega + \frac{2\pi D_v \delta_g t}{\Omega S n_{\text{vsp}}} \right) \left(\frac{\delta C}{3N_{\text{sp}}} \right) \right]^{2/3} \left(\frac{2}{3a^{1/3}} \right) \quad (11)$$

299 in which it is neglected that the proposed N_{lim} depends on the grain size itself Eq. (7). Eq.
 300 10 points out a dependence of the *FGR* to the rod free volume of $a^{2/3}$. This effect is due to
 301 the decrease of the surface-to-volume ratio of the grain with the increase of the grain radius
 302 a . Looking at the derivative (Eq. 11) one can observe that this process is limited since the
 303 $\partial \delta n_{\text{FGR}} / \partial a$ follows a law proportional to $a^{-1/3}$. Hence, with larger grains, the surface-to-
 304 volume ratio decreases and this increases grain boundary storing capacity. When many gas
 305 atoms are stored in the grain boundaries, the release does not depend on the intra-granular
 306 diffusion anymore (Eq. 9) but just on the law described in Eq. 10. This can happen just
 307 when many gas atoms are stored in the grain boundaries, and only after a certain burnup
 308 level. As the release threshold is reached, there is an expected impact of the proposed N_{lim}
 309 value on the concentration of gas being released. This impact is quantitatively evaluated
 310 by considering the variation of N_{lim} with the grain size a , namely:

$$\frac{\partial N_{\text{lim}}}{\partial a} = - \frac{n_{\text{eq,lim}} n_{\text{face}}}{4\pi a^3} \quad (12)$$

311 After the lower bound to the inter-granular bubble number density is reached, the
 312 coalescence process described by Eq. 3 is considered to stop. This calls for a different
 313 expression of the linearized equations governing the grain boundary gas behaviour, resulting
 314 in

$$\delta n_{\text{FGR}} = \frac{n_{\text{sp}}}{A_{\text{sp}}} \left[\left(\omega + \frac{2\pi D_v \delta_g t}{\Omega S n_{\text{vsp}}} \right) \left(\frac{\delta C}{3N_{\text{sp}}} a \right) \right]^{2/3} N_{\text{lim}} \quad (13)$$

$$\frac{\partial \delta n_{\text{FGR}}}{\partial a} = \frac{n_{\text{sp}}}{A_{\text{sp}}} \left[\left(\omega + \frac{2\pi D_v \delta_g t}{\Omega S n_{\text{vsp}}} \right) \left(\frac{\delta C}{3N_{\text{sp}}} \right) \right]^{2/3} \left(\frac{2}{3} a^{2/3} \right) \frac{\partial N_{\text{lim}}}{\partial a} \quad (14)$$

315 Thus after the lower bound $N = N_{\text{lim}}$ is reached, there is an impact of the proposed
 316 model parameter on the overall fission gas release. By comparing Eqs. 11 and 14, we can
 317 observe that

- The amount of gas released from the grain boundaries is proportional to the proposed lower bound for the bubble density (considering a linear approximation of model equations). Higher values used for this parameter, e.g., considering higher number of bubbles per grain face or higher number of faces per grain, hence imply a higher predicted fission gas release.
- The dependency on the grain size of the proposed lower bound, expressed by Eq. 12, implies that the expected dependency of the fission gas release on the grain radius changes after the lower bound is reached.

Since the grain radius a is the only free parameter involved in the definition of the lower bound N_{lim} , we reported in Table 2 the dependency of the discussed figures of merit on the grain radius itself, clarifying the change in dependency between the predicted fission gas release with/without considering any lower bound (i.e., after/before the lower bound is eventually reached). It is worth noting that after the lower bound is reached, the predicted fission gas release becomes monotonically decreasing with the grain radius since higher grain radius correspond to lower values of the proposed lower bound (Eq. 7).

Table 2: Summary of the sensitivity analysis about the dependency on the grain radius for intra-granular and inter-granular behaviour.

Scenarios	Figure of merit	Dependency on grain radius, a
Intra-granular behaviour	Variation of intra-granular gas concentration, δC	$\delta C \sim a^{-1}$
Inter-granular behaviour w/o proposed limit	Variation of fission gas released, δn_{FGR}	$\delta n_{\text{FGR}} \sim a^{2/3}$
Inter-granular behaviour w/ proposed limit	Variation of fission gas released, δn_{FGR}	$\delta n_{\text{FGR}} \sim a^{-4/3}$

After this analytical study, we also investigated the effect of the grain-size on the results performing additional simulations. Fig. 6 shows a comparison between the case using the current version of BISON and the one with N_{lim} proposed in this work, also considering two different constant values of grain radius: 5 and 10 μm for the L09 pin; 4 and 8 μm for MK-I and MK-II cores. These values lie in the range that goes from 4 to 10 μm referred to a realistic size for the grain characteristic dimension after the restructuring (Ainscough et al. [32]). Looking at Fig. 6, one can make some observations.

- The FGR for the cases using the limitation N_{lim} with a lower grain radius (black line) is higher than in the case with a higher grain radius (blue line). A smaller grain leads to a shorter average diffusion path to the grain boundary. Hence, due to this intra-granular diffusion effect (Eq. 1), in a smaller grain, more gas atoms will reach the grain boundary and will be released. This effect can be easily observed also in Table 2. In this table, we report the dependency on the grain radius for both the behaviours (intra-granular and inter-granular).
- In Figs. 6a-6b the intra-granular diffusion effect (Eq. 9) prevails again (red line versus purple line) on the surface-to-volume effect described for the grain boundary gas behaviour (Eq. 10), see also Table 2. Hence, in a smaller grain, more gas can

350 reach the grain boundary and then can be released. However, Fig. 6c shows that
 351 this is valid only until a certain value of burnup (the purple line crosses the red one).
 352 After a certain burnup level, the grain boundary storing capability becomes dominant:
 353 many gas atoms are already stored in the grain boundary and ready to be released.
 354 As shown by Eq. 10, this storing capability is improved with larger grains.

- 355 • Again up to a certain burnup (approximately $\sim 1.5\%$ FIMA) the case with N_{lim} with
 356 a larger grain (blue line) has a lower release compared to the case with no limita-
 357 tions and with a smaller grain (red line). This shows that up to that burnup the
 358 intra-granular effect is stronger, but beyond the grain boundary storing capacity be-
 359 comes the dominant effect. Furthermore, one can notice that the approaching of the
 360 bubble number density lower limit, where (from Eq. 7) it corresponds to a value of
 361 2×10^{11} bubbles m^{-2} , improves the release for the case represented by the blue line.
 362 Consequently, once the lower limit for the number density of bubbles is achieved, any
 363 further bubble growth is compensated by FGR. This is shown in Fig. 6a and Fig. 6c,

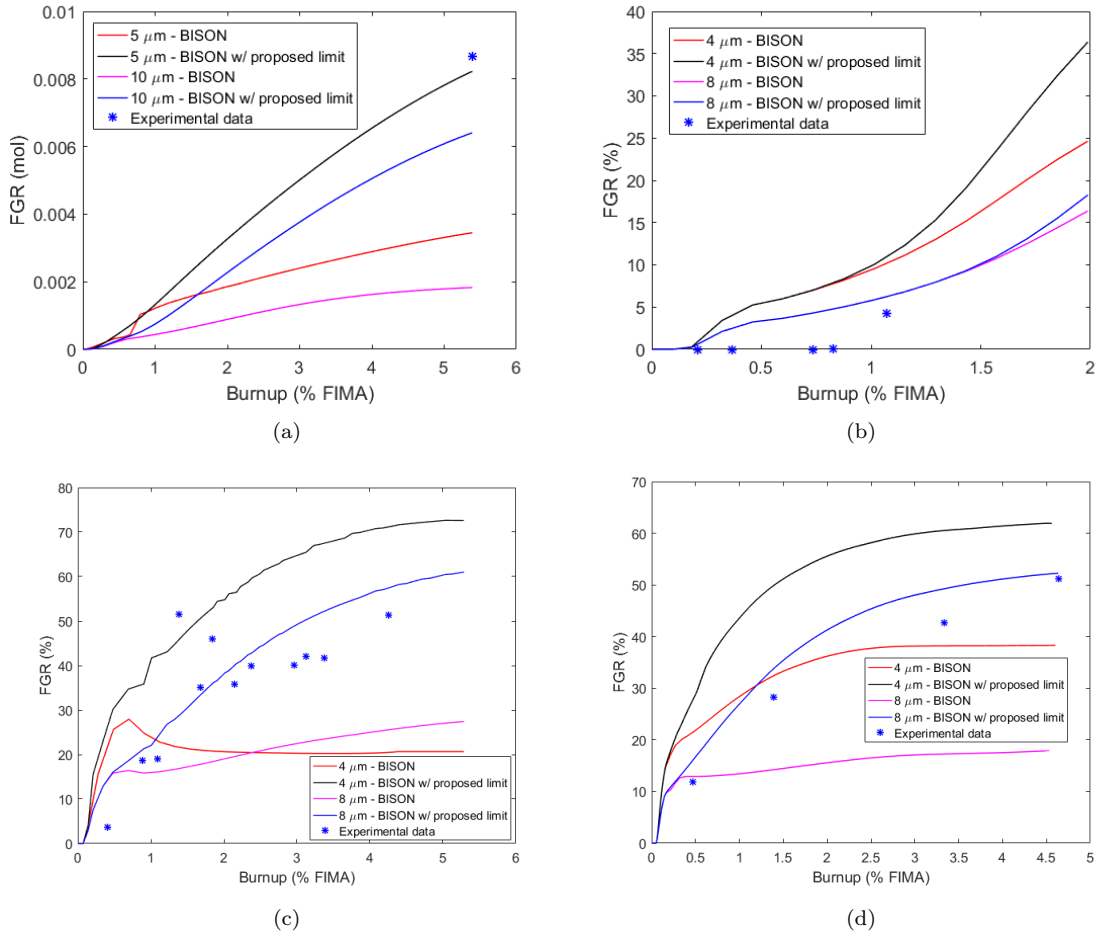


Figure 6: Sensitivity analysis performed varying the grain radius in a realistic range after the restructuring (from 4 to 10 μm). Fig. 6a refers to the fuel pin L09 from the FO-2 assembly (grain radius of 5 and 10 μm , with N_{lim} corresponding to 2×10^{11} and 5.5×10^{10} bubbles m^{-2} , respectively); Figs. 6b-6c show the sensitivity analysis for MK-I core irradiated at 50 MW_t and at 75 MW_t respectively, while the simulations for MK-II core are illustrated in Fig. 6d (grain radius of 5 and 10 μm , with N_{lim} corresponding to 3.5×10^{11} and 8.7×10^{10} bubbles m^{-2} , respectively).

364

while in Fig. 6b a sufficiently high level of burnup is not reached.

365

6. Conclusion and future work

366

The main goal of this work was modelling fission gas behaviour in fast reactor (U,Pu)O₂ fuel with BISON. A model for the calculations of fission gas behaviour was already included in BISON. However, this model was validated only for LWR cases so far. We proposed a new physics-based limit to represent conditions of extended bubble growth and interlinkage at grain boundaries that occur at high temperatures (typical conditions achieved during irradiation in FBRs). Therefore, the scope of this work is to show that a model for fission gas behaviour developed for LWR conditions with few improvements could have a good reproducibility of the results for (U,Pu)O₂ irradiated in fast reactors. However, we are aware that many other phenomena that affect FGR (like stoichiometry, Plutonium content, species migration) are relevant and they should be considered in future work. We applied the extended model to local simulations (i.e., performed using a simplified fuel-only model with a single-cube mesh) in order to prove the importance of the limit. Hence, we applied the model to integral FBR (U,Pu)O₂ fuel rod simulations with BISON demonstrating a marked improvement in the FGR predictions compared to the standard version of BISON. In particular, the results point out that at low temperatures the grain-face bubble growth and the consequent coalescence are far from their physical limits, while at higher ranges those limiting effects occur. Also, the sensitivity analysis performed highlights the strong dependency of the FGR on the grain size. In conclusion, according to the results obtained in this work, the extension to the fission gas behaviour model provides an improved representation of fission gas behaviour under fast reactor conditions. Future efforts can be invested in the validation of the proposed model against more irradiation cases, and in the analysis of other kinds of (U,Pu)O₂ fuels as well. For example, the model could be improved taking into account the heterogeneity effect of the MOX fuels, due to the presence of plutonium agglomerates, on the fission gas release. This feature becomes very important in the modelling of MOX fuel irradiated in thermal reactors. This could be done implementing into the present model the outcomes from the studies of Koo et al. [12] and of Ishida and Korei [37].

393

A further perspective for future work regards the effect of open porosity to the release. The model describes the release by point, but it could be improved to consider also inner surfaces due to the formation of a central void or because the fuel pin is annular.

396

Another open issue is the development of a grain growth model able to describe better this phenomenon at high temperatures, especially after the restructuring in order to define also the columnar grain region. So far, all the grains have been considered as spheres, but this approximation can be valid only for as-fabricated and equiaxed grain regions. The columnar grains, instead, present a cylindrical shape, hence, in this case, all the equations involved should be described with cylindrical coordinates. This improvement could be also useful for the sensitivity analysis prospect because a grain growth model can feed directly the expression presented in this work for the N_{lim} , which can be adopted for a more accurate sensitivity analysis. However, the sensitivity analysis is not the main goal of this work, and this study will be investigated more deeply in future work, taking into account other parameters and phenomena besides the grain size.

406

407 **7. Acknowledgements**

408 This work involved a collaboration between the Nuclear Reactors Group of the Depart-
409 ment of Energy of Politecnico di Milano and the BISON team of Idaho National Laboratory
410 (INL), in the framework of the I-NERI initiative. It has been funded by the U.S. Depart-
411 ment of Energy – Nuclear Energy Office (DOE-NE) and by the Advanced Fuel Campaign
412 (AFC) of the Nuclear Technology Research and Development Program. The authors are
413 grateful to Mr R. Genoni for his help in generating the sample images for the study of the
414 bubble equivalent number. This manuscript has been authored by a contractor of the U.S.
415 Government under Contract DE-AC07-05ID14517.

416 **References**

- 417 [1] A. Waltar, D. Todd, P. Tsvetkov, *Fast Spectrum Reactors*, Springer, 2012.
- 418 [2] B. Merk, A. Stanculescu, P. Chellapandi, R. Hill, Progress in reliability of fast reactor
419 operation and new trends to increased inherent safety, *Applied Energy* 147 (2015)
420 104–116.
- 421 [3] D. R. Olander, *Fundamental aspects of nuclear reactor fuel elements*, Technical Infor-
422 mation Center, Energy Research and Development Administration, 1976.
- 423 [4] S. Fisher, R. White, P. Cook, S. Bremier, R. Corcoran, R. Stratton, C. Walker, P. Ivi-
424 son, I. Palmer, Microstructure of irradiated SBR MOX fuel and its relationship to
425 fission gas release, *Journal of Nuclear Materials* 306 (2002) 153 – 172.
- 426 [5] K. Maeda, K. Katsuyama, T. Asaga, Fission gas release in FBR MOX fuel irradiated
427 to high burnup, *Journal of Nuclear Materials* 346 (2) (2005) 244 – 252.
- 428 [6] I. Sato, K. Katsuyama, Y. Arai, Fission gases and helium gas behavior in irradiated
429 mixed oxide fuel pin, *Journal of Nuclear Materials* 416 (2011) 151–157.
- 430 [7] R. Parrish, A. Aitkaliyeva, A review of microstructural features in fast reactor mixed
431 oxide fuels, *Journal of Nuclear Materials* (2018).
- 432 [8] S. Novascone, P. Medvedev, J. W. Peterson, Y. Zhang, J. Hales, Modeling porosity
433 migration in LWR and fast reactor MOX fuel using the finite element method, *Journal*
434 *of Nuclear Materials* 508 (2018) 226 – 236.
- 435 [9] F. Nichols, [Transport phenomena in nuclear fuels under severe temperature gradients](https://doi.org/10.1016/0022-3115(79)90147-8),
436 *Journal of Nuclear Materials* 84 (1) (1979) 1 – 25. doi:[https://doi.org/10.1016/](https://doi.org/10.1016/0022-3115(79)90147-8)
437 [0022-3115\(79\)90147-8](https://doi.org/10.1016/0022-3115(79)90147-8).
438 URL <http://www.sciencedirect.com/science/article/pii/0022311579901478>
- 439 [10] M. Welland, Matter transport in fast reactor fuels, *Comprehensive Nuclear Materials*
440 3 (2012) 629–676. doi:[10.1016/B978-0-08-056033-5.00073-2](https://doi.org/10.1016/B978-0-08-056033-5.00073-2).
- 441 [11] R. J. Parrish, F. Cappia, A. Aitkaliyeva, [Comparison of the radial effects of burnup on](https://doi.org/10.1016/j.jnucmat.2020.152003)
442 [fast reactor mox fuel microstructure and solid fission products](https://doi.org/10.1016/j.jnucmat.2020.152003), *Journal of Nuclear Ma-*
443 *terials* 531 (2020) 152003. doi:<https://doi.org/10.1016/j.jnucmat.2020.152003>.
444 URL <http://www.sciencedirect.com/science/article/pii/S0022311519313297>

- 445 [12] Y.-H. Koo, B.-H. Lee, J.-S. Cheon, D.-S. Sohn, Modeling and parametric studies of
446 the effect of inhomogeneity on fission gas release in LWR MOX fuel, *Annals of Nuclear*
447 *Energy* 29 (3) (2002) 271 – 286.
- 448 [13] L. Luzzi, A. Cammi, V. D. Marcello, S. Lorenzi, D. Pizzocri, P. V. Uffelen, Application
449 of the TRANSURANUS code for the fuel pin design process of the ALFRED reactor,
450 *Nuclear Engineering and Design* 277 (2014) 173–187.
- 451 [14] INSPYRE.
452 URL <http://www.eera-jpnm.eu/inspyre/>
- 453 [15] Generation IV International Forum.
454 URL https://www.gen-4.org/gif/jcms/c_9261/home
- 455 [16] Fuel Cycle Research & Development.
456 URL [https://www.energy.gov/ne/fuel-cycle-technologies/
457 fuel-cycle-research-development](https://www.energy.gov/ne/fuel-cycle-technologies/fuel-cycle-research-development)
- 458 [17] G. Pastore, L. Luzzi, V. D. Marcello, P. V. Uffelen, Physics-based modelling of fission
459 gas swelling and release in UO₂ applied to integral fuel rod analysis, *Nuclear Engineer-*
460 *ing and Design* 256 (2013) 75 – 86.
- 461 [18] G. Pastore, L. Swiler, J. Hales, S. Novascone, D. Perez, B. Spencer, L. Luzzi, P. V.
462 Uffelen, R. Williamson, Uncertainty and sensitivity analysis of fission gas behavior in
463 engineering-scale fuel modeling, *Journal of Nuclear Materials* 456 (2015) 398 – 408.
464 doi:<https://doi.org/10.1016/j.jnucmat.2014.09.077>.
- 465 [19] R. L. Williamson, J. D. Hales, S. R. Novascone, M. R. Tonks, D. R. Gaston, C. J.
466 Permann, D. Andrš, R. C. Martineau, Multidimensional multiphysics simulation of
467 nuclear fuel behavior, *Journal of Nuclear Materials* 423 (1–3) (2012) 149–163.
- 468 [20] C. Baker, The migration of intragranular fission gas bubbles in irradiated uranium
469 dioxide, *Journal of Nuclear Materials* 71 (1) (1977) 117 – 123. doi:[https://doi.org/
470 10.1016/0022-3115\(77\)90195-7](https://doi.org/10.1016/0022-3115(77)90195-7).
- 471 [21] C. Baker, The fission gas bubble distribution in uranium dioxide from high temperature
472 irradiated SGHWR fuel pins, *Journal of Nuclear Materials* 66 (3) (1977) 283 – 291.
473 doi:[https://doi.org/10.1016/0022-3115\(77\)90117-9](https://doi.org/10.1016/0022-3115(77)90117-9).
- 474 [22] C. W. J.A. Turnbull, R.J. White, The diffusion coefficient for fission gas atoms in
475 uranium dioxide, IAEA-TC-699/3.5 (1988).
- 476 [23] M. V. Speight, [A calculation on the migration of fission gas in material exhibiting
477 precipitation and re-resolution of gas atoms under irradiation](#), *Nuclear Science and En-*
478 *gineering* 37 (2) (1969) 180–185. arXiv:<https://doi.org/10.13182/NSE69-A20676>,
479 doi:[10.13182/NSE69-A20676](https://doi.org/10.13182/NSE69-A20676).
480 URL <https://doi.org/10.13182/NSE69-A20676>
- 481 [24] M. V. Speight, W. B. Beeré, Vacancy potential and void growth on grain boundaries,
482 in: *Metal Science*, Vol. 9, 1975, p. 131–140.
- 483 [25] R. White, The development of grain-face porosity in irradiated oxide fuel, *Journal of*
484 *Nuclear Materials* 325 (1) (2004) 61 – 77.

- 485 [26] R. Williamson, K. Gamble, D. Perez, S. Novascone, G. Pastore, R. Gardner, J. Hales,
486 W. Liu, A. Mai, Validating the bison fuel performance code to integral lwr experiments,
487 Nuclear Engineering and Design 301 (2016) 232–244. doi:[10.1016/j.nucengdes.](https://doi.org/10.1016/j.nucengdes.2016.02.020)
488 [2016.02.020](https://doi.org/10.1016/j.nucengdes.2016.02.020).
- 489 [27] T. Barani, E. Bruschi, D. Pizzocri, G. Pastore, P. V. Uffelen], R. Williamson,
490 L. Luzzi, [Analysis of transient fission gas behaviour in oxide fuel using BISON and](https://doi.org/10.1016/j.jnucmat.2016.10.051)
491 [TRANSURANUS](https://doi.org/10.1016/j.jnucmat.2016.10.051), Journal of Nuclear Materials 486 (2017) 96 – 110. doi:[https:](https://doi.org/10.1016/j.jnucmat.2016.10.051)
492 [//doi.org/10.1016/j.jnucmat.2016.10.051](https://doi.org/10.1016/j.jnucmat.2016.10.051).
493 URL <http://www.sciencedirect.com/science/article/pii/S002231151630544X>
- 494 [28] J.-Y. Colle, J.-P. Hiernaut, T. Wiss, O. Beneš, H. Thiele, D. Papaioannou,
495 V. Rondinella, A. Sasahara, T. Sonoda, R. Konings, Fission product release and mi-
496 crostructure changes of irradiated MOX fuel at high temperatures, Journal of Nuclear
497 Materials 442 (1) (2013) 330 – 340.
- 498 [29] P. C. Millett, M. R. Tonks, S. Biner, L. Zhang, K. Chockalingam, Y. Zhang, [Phase-](https://doi.org/10.1016/j.jnucmat.2011.07.034)
499 [field simulation of intergranular bubble growth and percolation in bicrystals](https://doi.org/10.1016/j.jnucmat.2011.07.034), Journal
500 of Nuclear Materials 425 (1) (2012) 130 – 135, microstructure Properties of Irradiated
501 Materials. doi:<https://doi.org/10.1016/j.jnucmat.2011.07.034>.
502 URL <http://www.sciencedirect.com/science/article/pii/S0022311511007458>
- 503 [30] L. K. Aagesen, D. Andersson, B. W. Beeler, M. W. Cooper, K. A. Gamble, Y. Miao,
504 G. Pastore, M. R. Tonks, [Phase-field simulations of intergranular fission gas bubble](https://doi.org/10.1016/j.jnucmat.2020.152415)
505 [behavior in u3si2 nuclear fuel](https://doi.org/10.1016/j.jnucmat.2020.152415), Journal of Nuclear Materials 541 (2020) 152415. doi:
506 <https://doi.org/10.1016/j.jnucmat.2020.152415>.
507 URL <http://www.sciencedirect.com/science/article/pii/S0022311520310230>
- 508 [31] J. Turnbull, C. Friskney, J. Findlay, F. Johnson, A. Walter, The diffusion coefficients
509 of gaseous and volatile species during the irradiation of uranium dioxide, Journal of
510 Nuclear Materials 107 (2) (1982) 168 – 184.
- 511 [32] J. Ainscough, B. Oldfield, J. Ware, Isothermal grain growth kinetics in sintered UO₂
512 pellets, Journal of Nuclear Materials 49 (2) (1973) 117 – 128.
- 513 [33] L. Gilpin, R. Baker, S. Chastain, Evaluation of the advanced mixed oxide fuel test
514 FO-2 irradiated in Fast Flux Test Facility, Westinghouse Hanford Co., Richland, WA
515 (USA), Annual meeting of the American Nuclear Society; Atlanta, GA (USA) 4-8 June
516 4-8, 1989.
- 517 [34] M. Teague, M. Tonks, S. Novascone, Microstructural modeling of thermal conductivity
518 of high burn-up mixed oxide fuel, Journal of Nuclear Materials 444 (1) (2014) 161 –
519 169.
- 520 [35] T. Shimada, T. Itaki, Y. Nara, Operational experience of experimental fast reactor
521 JOYO driver fuel, International Conference on Reliable Fuels for Liquid Metal Reac-
522 tors, 1986.
- 523 [36] A. Karahan, Modeling of thermo-mechanical and irradiation behavior of metallic and
524 oxide fuels for sodium fast reactors, Ph.D. thesis, Massachusetts Institute of Technol-
525 ogy, <https://tinyurl.com/y72vqvbn> (Jun. 2009).

- 526 [37] M. Ishida, Y. Korei, Modeling and parametric studies of the effect of pu-mixing het-
527 erogeneity on fission gas release from mixed oxide fuels of LWRs and FBRs, Journal of
528 Nuclear Materials 210 (1) (1994) 203 – 215.